Science Arts & Métiers (SAM)

is an open access repository that collects the work of Arts et Métiers Institute of Technology researchers and makes it freely available over the web where possible.

This is an author-deposited version published in: https://sam.ensam.eu
Handle ID: .http://hdl.handle.net/10985/17659

To cite this version :

Hassan ZAHOUANI, Mohamed EL MANSORI - Multi-scale and multi-fractal analysis of abrasive wear signature of honing process - Wear - Vol. 376-377, p.178-187 - 2017

Any correspondence concerning this service should be sent to the repository Administrator : scienceouverte@ensam.eu

Arts et Métiers Institute of Technology

Multi-scale and multi-fractal analysis of abrasive wear signature of honing process

H. Zahouani [a,*], M. EL Mansori [b]

[a] Laboratory of Tribology and Dynamic of Systems, University of Lyon, ENISE- ECL-ENTPE, UMRS CNRS 5513, 36, Avenue Guy de Collongue, 69131 Ecully Cedex, France
[b] MSMP-EA7350, Arts et Métiers ParisTech, Rue Saint Dominique, BP 508, 51006 Châlons-en-Champagne, France

A B S T R A C T

Honing is an industrial alternative of internal grinding for finishing large-diameter bores of internal combustion engine cylinders. This paper introduces a hybrid approach for a multi-scale analysis of surface finish in abrasive honing. The methodology is based on morphological identification of scratch pattern of manufactured surfaces, produced at various honing conditions, and their 2D continuous wavelet decomposition. The activated abrasion mechanisms were then discussed based on quantitative analysis of geometrical scratch pattern and multi-scale surface modifications of honing signature. Results show clearly that honed surface finish is primarily controlled by the size and the geometry of abrasive grains (i.e. wear of abrasive sticks). Since the abrasive is in continuous balanced contact with the work in honing operating at constant-force grinding, there is less deflection of the work. Moreover, it appears that honing signature shows a multi-scale fractal structure along the observation scales. This makes it possible to identify an optimal honing route preserving honing sticks abrasiveness and increasing their texturing capacity to confer high volume of oil retention at honed surface finish.

Keywords:
Abrasion
Honing process
Morphological decomposition
Continuous wavelet transform
3d motifs
multi-fractal
Archard' Law

1. Introduction

Cylinder liner surface roughness has shown a large impact on friction and oil consumption and many conventional and non-conventional liner surface finishes have been, and are being developed with the aim to reduce friction losses and oil consumption. Satisfactory improved surface specifications are often composed of specialized functional surface parameters, narrow in parameter tolerances creating higher demands on a consistent and controlled surface roughness quality in manufacturing of cylinder liners, and especially the honing of the cylinder liner surface.

Cast iron is the most common material cylinder liners. Grey cast iron is tribologically beneficial as the graphite phase of the material gives a dry lubrication effect. The most common process for manufacturing of liner surfaces is honing. Honing is an abrasive process where the material is removed from the work piece using irregularly shaped abrasive grains.

Historically honing of cylinder liner surfaces was done in one step leaving of coarse surface with enough material left to be worn off during run in of the engine itself and leave a surface with smoothened and some valleys left to contain lubrication oil. Today honing of cylinder liner surfaces is done in several steps with the aim to imitate a perfectly run in engine. This pre run-in is accomplished in the last stage of the manufacturing by reducing the upper portions of the surface using more gentle honing with reduced surface pressure or manufacturing with fine sized grains.

The finishing of the cylinder liner surface results in a crisscross patterned topography consisting of a series of honing valleys of different angle, density, depth and widths related to selected machining parameters (speed, feed and surface pressure) along with selection of honing tool composition of grain size, grain material (diamond or SiC), binding material and grain density.

An abrasive finishing process is considered as a complex process during which a hard abrasive scratch an opposing surface of a softer material, generating a plastic surface modification [1–5]. The abrasive grain has a plurality of cutting edges and faces of different geometries and dimensions with different modes of inducing stresses and deformation [6–9].

Depending on the attack angle we can classify different modes of abrasion:

- Abrasion Mode I type Ploughing: It is characterized by the appearance of a bead groove head. No debris from coming loose during the process and the residual trace is defined as a plastic groove;
- Abrasion Mode II: plastic piling-up: forming side piling-up and a plastic corner remains in front of the contact
- Abrasion Mode III cutting type: It is defined by the formation of

* Corresponding author.
E-mail address: hassan.zahouani@ec-lyon.fr (H. Zahouani).

a micro-chip. The flat surface to the tip is deformed first and then form a micro-chip. This process is similar to a machining tool with a negative attack angle. The cutting mode is regularly represented by abrasion as a degeneration of ploughing mode;
– Abrasion Mode IV Fragmentation types: It is characterized by the appearance of cracks as piling back the tip. This mode is related to the nature of abraded material.

1.1. Influence of process variables in honing

The variables of the honing process can be classified as [10,11,12]:

1. Machine Variables: contact pressure, cutting speed, running time;
2. Variables tool (support stones): stiffness, stability;
3. Stone Variables: grain size, concentration, type of grain, type of binder;
4. Piece Variables: hardness, roughness, shape.

It is obvious that this distribution of parameters is only a simplified photography process. Honing involves, in fact, quite complex interactions between variables process. Moreover, the expertise of the automotive manufacturers for honing process is based on cards set from test series listed for different functional applications.

Chang et al. attempted to determine the interactions between influence parameters in finishing processes involving a wide range of oscillation combinations of speed and contact pressure with constant speed [12]. They then synthesized the results in the form of process map connecting the contact pressure to the oscillation of the stones. This map identifies four areas as follows:

– Zone I defining an effective cutting area of the stone. It is characterized by a high material removal rate, a significant roughness but low specific energy consumption;
– Zone II corresponds to a ploughing area resulting in a low rate of material removal, low roughness at the cost of high specific energy;
– So-called transition zone III where the process performance is random;
– Zone IV identified as a critical area where there is an increase in the thermal effects associated with specific energy higher because of the predominance of the friction phenomenon.

Other experimental approaches have been developed to identify these interactions localized at the interface abrasive tool/work piece in conjunction with process variables during follow-up of the surface finish.

The machine parameters essentially define the kinematics of the process and the contact conditions abrasive tool / piece. The running-in cutting speed "VC" is defined by the resultant of the rotational speed "*Vr*" and the axial velocity of the tool "*Va*", Fig. 1. It is determined by the following equation:

$$V_C = \sqrt{V_r^2 + \quad V_a} \tag{1}$$

1.2. Model of the abrasive particle

In the case where the geometry of an abrasive is close to a cone with an apex angle of 2 α, the average contact pressure is linked to the plastic elastic quantities E and Y by the equation:

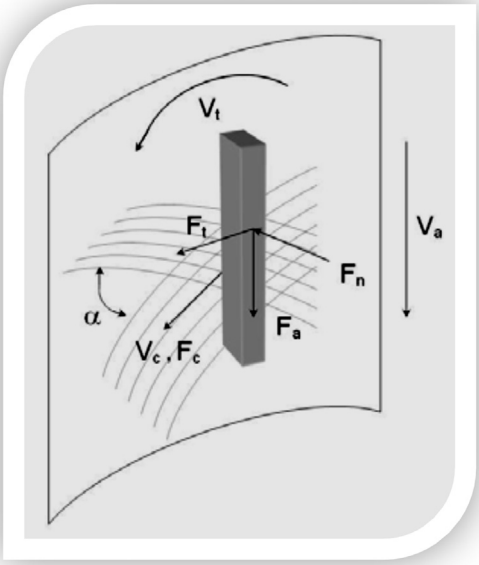

Fig. 1. The running-in cutting speed.

$$\frac{\bar{p}}{Y} = \quad \frac{2}{3}\left[ln\left(\frac{1}{3}\frac{Ecot\alpha}{Y} \right) \right] \tag{2}$$

Where $\bar{p}$ is the mean pressure, Y the yield stress (or yield to a deformation of 0.2%), E the elastic modulus of the piece. This relationship introduces the parameter $\frac{E}{Y}cot\alpha$, defining the relationship between the amount of strain imposed by the abrasive grain $cot\alpha$ and that the material can withstand before flowing plastically Y/E. In other words, this relationship can also be written as a function of the attack angle:

$$X = \frac{E}{Y}tg\beta \tag{3}$$

Where β is the attack angle of abrasive grain, X has the meaning of a plasticity index, if X is close to 1, the elastic return after indentation is very marked. If X is greater than 100, the deformation is essentially plastic [13] (Fig. 2).

If one is interested in the plowing component of friction, its expression is a function of the angle of attack of the abrasive grain [13]:

$$\mu_{pl} = \quad \frac{2}{\pi}Cot\alpha = \frac{2}{\pi}tg\beta \tag{4}$$

One can introduce a parameter that takes into account the geometry of the abrasive grain to define the severity of the deformation. In the case of the abrasion by a single particle, it creates three possible types of deterioration: plastic plowing, wedge and

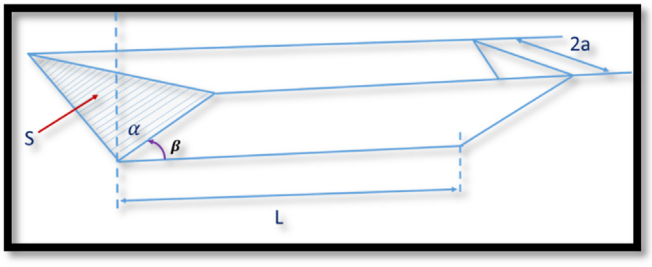

Fig. 2. Model of a single abrasive grain.

the chip. To determine the severity of this deformation, it is useful to introduce a distortion parameter ε_{def}, which characterizes the degree of penetration and which is defined as:

$$\varepsilon_{def} \approx \frac{\rho}{a} \tag{5}$$

Where ρ is the penetration depth.

For a lubricated interface, the plastic plowing is obtained if $\varepsilon_{def} < 0.1$ [39].

1.3. Characteristic parameters of abrasion

1.3.1. Abraded volume

During the sliding of an abrasive particle, the abraded volume per unit distance is defined as [14]:

$$V_{abr} = \frac{L\,S}{L} = S \tag{6}$$

Where:

L: sliding distance

S: cross section of the groove

This expression results in:

$$V_{abr} = \frac{a^2}{tg\alpha} \tag{7}$$

Where a is the contact radius.

According to Archard, there is however a big difference between friction and wear; ie, if all contacts contribute to friction, only a small portion, however, contribute to wear. This means that a proportion K contributes to wear. This proportion corresponds to the solicited contacts and providing wear particles. According to Archard, K varies between $\mathbf{10^{-2}}$ and $\mathbf{10^{-7}}$. Archard therefore concludes that the asperity should rub numerous times before emitting a particle.

Thus the asperity first undergo plastic deformation and then many elastic deformation before breaking. Only a very small proportion K participates to wear, in this case the wear rate of abrasion is defined as [14]:

$$V_{abr} = KA_r \tag{8}$$

Where:

A_r is the real contact area

K: is the wear coefficient ($K < 1$)

The real contact area between rough body may be the sum of many small contact areas. If a is the dimension of one of the spots and their number n:

$$A_r = n\,a \tag{9}$$

if there is a large number of small areas, the static theory of hardness indicates than the actual area of contact is proportional to the normal force F_z, the coefficient being the hardness of the softer material H:

$$F_z = A_r H \tag{10}$$

Taking into account the above relations, we get:

$$V_{abr} = K\frac{F_z}{H} \tag{11}$$

1.3.2. The characteristic contact time

In the process of finishing of surfaces by abrasion, one can define two characteristic times: i) the duration of the contact time : $t_c = \frac{2a}{V}$. ii) The time until the heat emitted from a point on a surface to reach a depth z = a. This time of heat diffusion is defined as: $t_d = \frac{a^2}{\xi}$

where ξ is the thermal diffusivity coefficient (m^2/s). For gray cast this study, the value of this coefficient is: 10^{-5} (m^2/s). The ratio of the heat diffusion time by the contact time can determine the Peclet number, ϕ [15]

$$\phi = \frac{t_d}{t_c} = \frac{V}{2a}\frac{a^2}{2\xi} = \frac{Va}{2\xi} \tag{13}$$

If $\phi < 0.2$, the heat source is considered quasi-static.

The parameters defined in this abrasion model, will be studied in detail in the experimental protocol to identify the effect of the abrasive honing on the quality of the finishing of cylinder liner.

2. Material and methods

This study aims to quantitatively analyze the quality of abrasion in the finishing of cylinder liner by honing process. Four honed surfaces by various process parameters will be studied to identify the quality of abrasion, Fig. 3. The Table 1 gives the specifications of the process conditions.

To understand the abrasion signature in the honing process, we are interested in characterizing the topography of the four-cylinder surfaces. The main objective is to identify the optimal finishing of honing through the topography of abrasive scratches and their multi-scale character, depending on process parameters. Two multi-scale approaches of characterization will be developed.

The first approach is based on a decomposition into three-dimensional patterns of the surface by identifying the local geometry of the local motif (amplitude, width, summit angle and attack angle), and anisotropy effect.

The second is based on the continuous multi-scale wavelet decomposition of surface topography of cylinders, the result will be presented as a function of the amplitude of the honing traces in a wide range of wavelengths.

The 3D topography of the different finished surface was measured by a white-light confocal microscope. Geometric traces printed during the process by honing, will be considered as a population of motifs similar to the deformation printed by a conical grain. In order to apply the theory of abrasion and determination of all the parameters in the previous paragraph that characterize the abrasion of conical geometry, we considered that the topographic signature process by honing as a population of motifs. Morphological analysis of the geometry of the patterns will be of great interest to establish a statistical analysis of honing effect

2.1. Motifs characterization of honing scratches

An interesting functional characterisation of surface topography can be performed using the MOTIF method (ISO 12085), but only from profiles. In this method, a 2D-motif is defined as the part of a profile between two peaks, Fig. 4 (two consecutive peaks defining an elementary motif) and significant motifs are obtained using combination rules.

The 3D extension of this method is interesting to study the finishing effect on surface topography. In this model, the 3D motif can be defined as the association of two summits separated with a pit [16]. The topological definition of summit and tip are given in Fig. 5.

Three parameters ρ, λ, θ, are necessary to define a three-dimensional linear motif: the depth ρ computed as the maximum difference between the summit and the pit:

$$\rho_{ij} = \left(Z_{\text{summit}}\right) - Z_{(\text{pit})} \tag{14}$$

the width of a 3D motif $\boldsymbol{\lambda}$ is defined as the Cartesian distance between two summits:

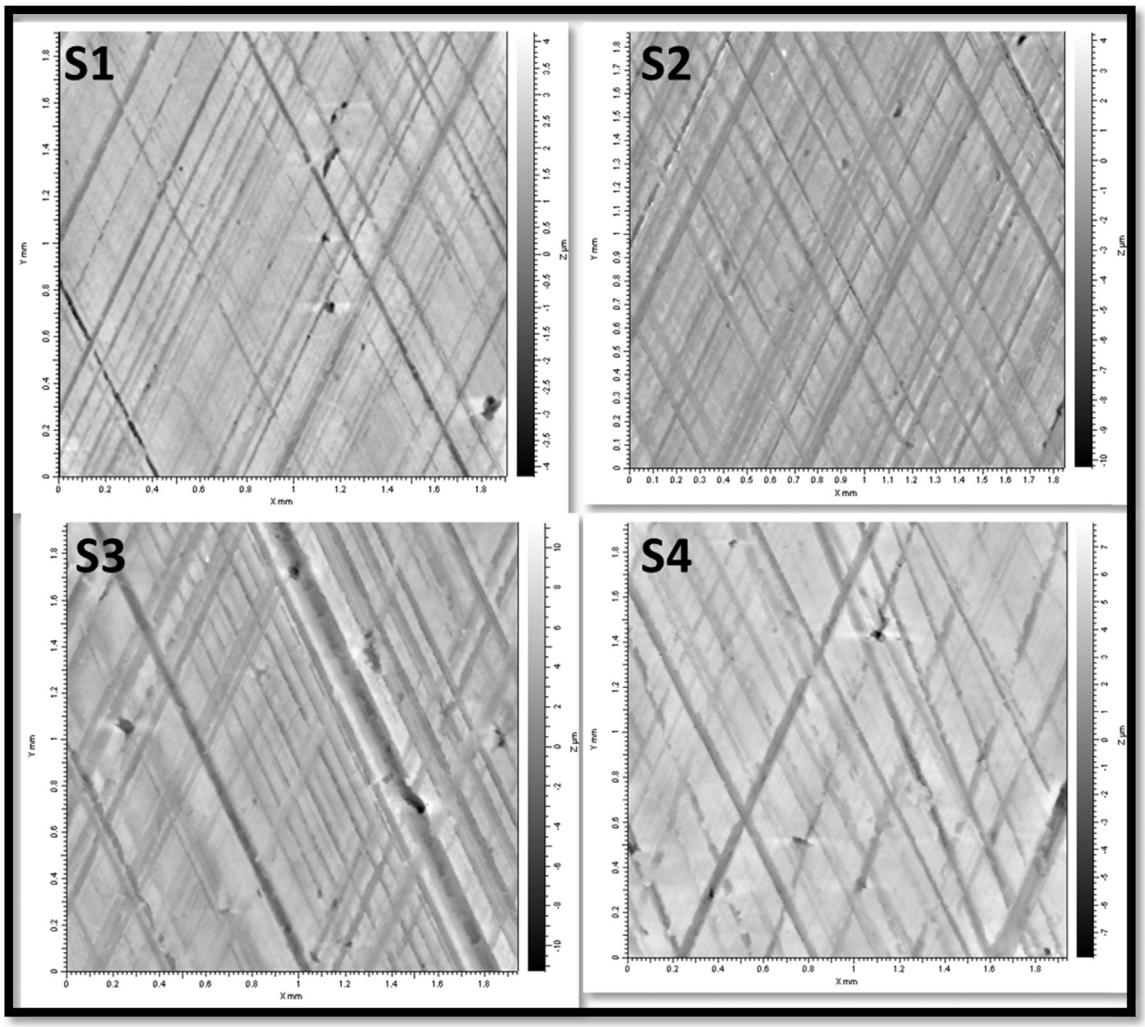

Fig. 3. Topography of honed surfaces.

Table 1
The experimental conditions [40].

Finished surface	Initial finishing: Grain size (μm) -V_c (m/min)	Second finishing: Grain size (μm) -V_c (m/min)	Contact pressure (bar)	Number of oscillations
S1	110 μm, V_c=50 m/min	30 μm, V_c=32 m/min	5 bars	5
S2	110 μm, V_c=50 m/min	0	5 bars	0
S3	110 μm, V_c=42.23 m/min	30 μm, V_c=42.23 m/min	5 bars	5
S4	110 μm, V_c=50 m/min	30 μm, V_c=50 m/min	2.5 bars	3.5

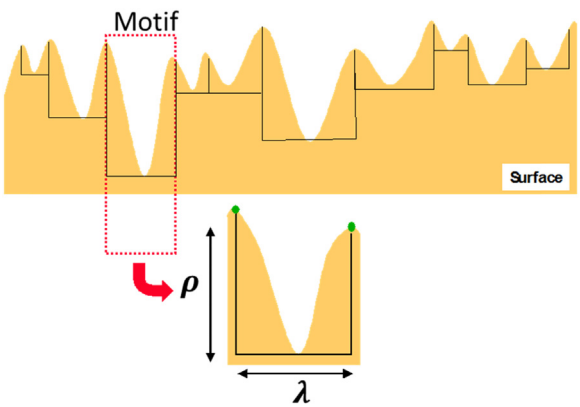

Fig. 4. Schematic diagram of 2D - motif.

$$\lambda = \sqrt{(x_2 - x_1)^2 + (y_2 - y_1)^2} \tag{15}$$

The direction θ of the motif is the orientation which coincides with the general direction of a principal manufacturing scratch or valley [17,18].

2.2. Application to the honing process

An example of quantitative analysis of geometrical patterns parameters is shown in the Fig. 6. Each parameter is statistically studied by determining density of distribution and the average value of each parameter. All of the quantitative results of abrasion parameters are summarized in Tables 2 and 3. It follows from this statistical analysis that the process parameters for the finishing of the surface S1 are best suited for finishing with less distortion, less

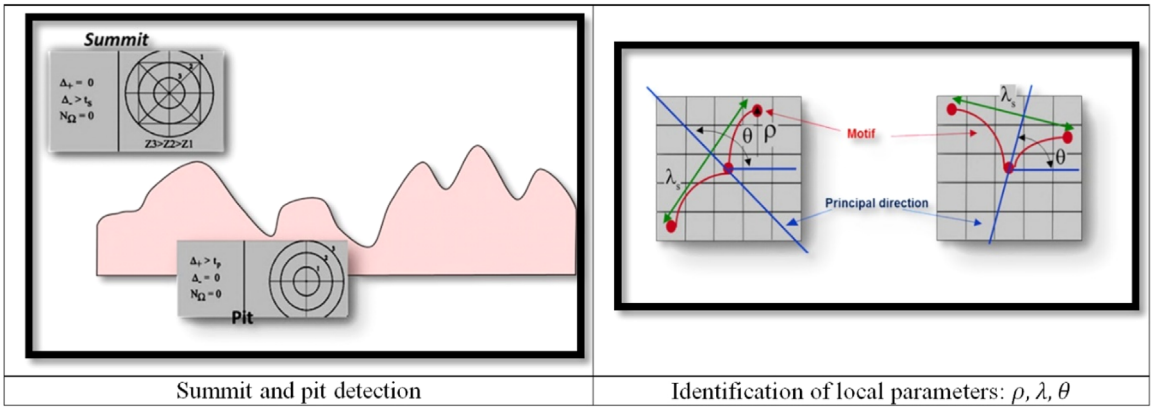

Fig. 5. Schematic diagram of 3D motif's definition.

wear, contact time and a number of lowest Peclet ϕ, which means diffusion of quasi-static heat, this shows the importance of cutting fluid role.

2.3. *Effect of the form of abrasive grain on plasticity index*

The plasticity index depends on the elastic properties of the material and geometry of the abrasive grain. The table below shows the plasticity index for the four honed surfaces

If X is close to 1, elastic return deformation is very marked. If X is greater than 100, the deformation is essentially plastic.

For conical geometry, the plasticity index X is defined as:

$$X = \frac{E}{Y} tg\beta \tag{16}$$

Based on the values calculated in the Table 4, the plastic deformation is primarily for large angles of attack ($\beta > 14$ °). For small angles of attack, the plasticity index decreases, but remains higher than 1. In this case the elastic return will be greater.

We also note that the plasticity index of the surface S1 is the

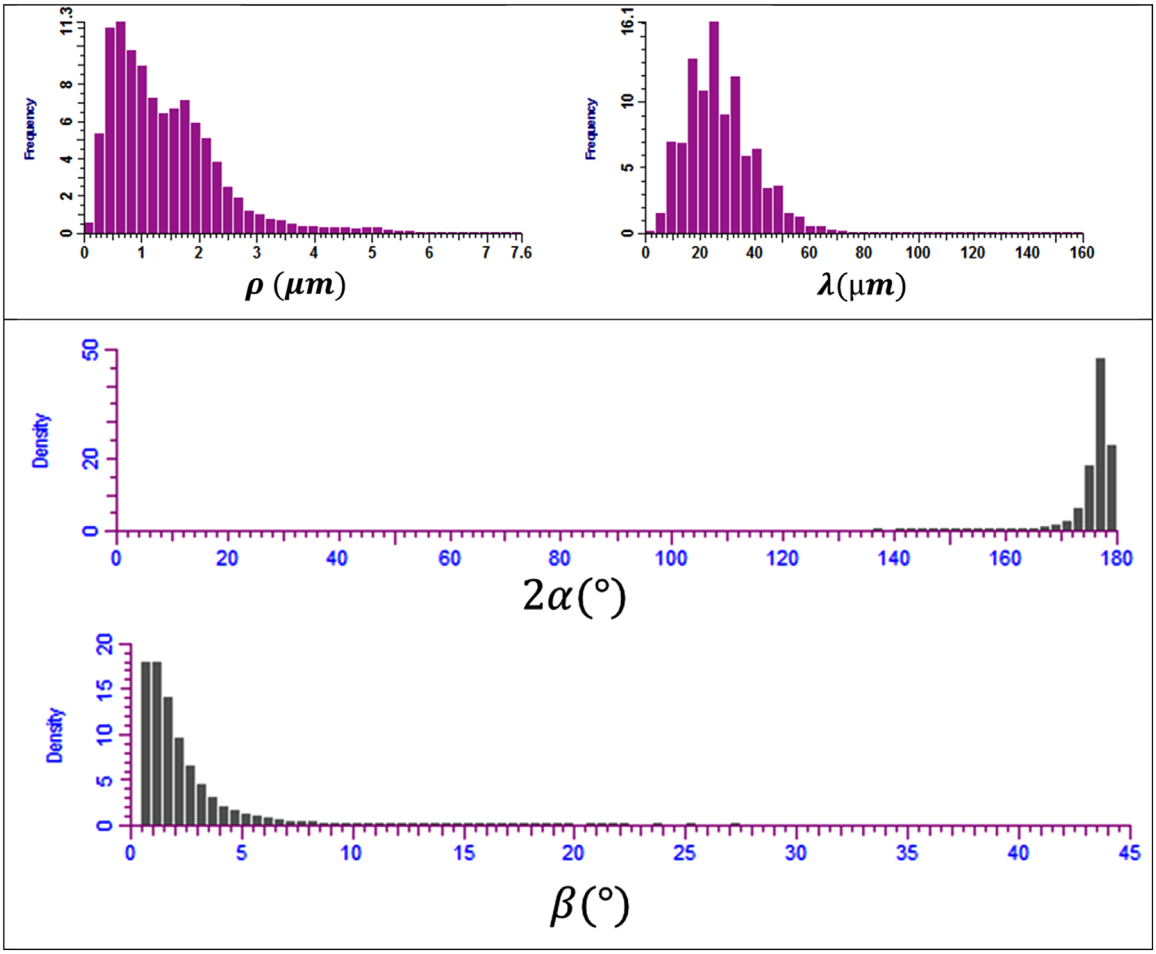

Fig. 6. Quantitative analysis of geometrical patterns.

Table 2
Quantitative parameters of abrasion.

Liner Surface	Number of motifs ($\times 10^4$)	ρ (μm)	$\lambda = 2a$ (μm)	$\frac{\rho}{a}$ ($\times 10^{-2}$)	$V_{abr}\left(x10^{-9}\right)\frac{m^3}{m}$	K ($\times 10^{-7}$)
S1	3	0.86	42.13	4	5.42	4.2
S2	2.6	1.34	40.34	6.6	7.02	8.02
S3	3.9	2.59	56.22	9.2	28.28	7.5
S4	2.64	1.46	50.9	5.75	9.8	6.9

Table 3
Quantitative parameters of time contact and heat diffusion.

Liner Surface	$t_c = \frac{2a}{v}\left(.10^{-5}\,s\right)$	$t_d = \frac{a^2}{\xi}(.10^{-6}.s)$,	$\phi=\frac{va}{2\xi}$ (10^{-3})
S1	7,9	0.43	5.4
S2	4.8	0.405	8.33
S3	8	0.79	9.87
S4	6.1	0.64	10.4

Table 4
Attack angles and plasticity index of different process.

Liner Surface	$\beta_{mean}(^\circ)$	β_{max} (°)	$X_{mean} = \frac{E}{Y}tg\beta_{mean}$	$X_{max} = \frac{E}{Y}tg\beta_{max}$
S1	1.7	21.66	11.87	158.5
S2	2.95	26.86	20.61	202.5
S3	3.4	36.81	23.76	299.34
S4	4.83	39.54	33.79	330

lowest, giving him signing as a homogeneous morphology.

2.4. Effect of honing angle on abrasive parameters

The texture of cylinder liner mainly consists of two sets of straight, approximately parallel grooves placed stochastically and appearing at different angles to the cylinder axis [19].

Honing angle is determined by the vertical and rotational movement of honing head with respect to the following formula:

$$\tan\left(\frac{\theta}{2}\right) = \frac{V_a}{V_r} \tag{17}$$

Where V_a is the axial speed and V_r is the rotation speed.

The honing angle is directly related to oil consumption and noxious emissions. Different studies and practical application have shown that oil consumption can be reduced by increasing honing angle [19].

The valleys component is intuitively associated to lubricant circulation and reservoirs. The prominence of the honing grooves suggests that they play an important role in the effect of surface texture on ring-pack performance.

The creation of two furrows families in two directions 65° and 135°, results in the creation of geometrically anisotropic motifs. To study the effect of anisotropy created by the process of running the abrasion parameters, we developed a new approach that takes into account the orientation of the pattern and determines the parameters studied in the previous paragraph, taking into account the orientation of the pattern.

Motif direction is achieved by the identification of the maximum local gradient variation. In fact, once the position (i,j) of a pit has been identified, we look for the two summits that corresponds to the maximum local variation in relief by working around the valley bottom in all directions. Two factors are used in this identification [18]:

The direction must coincide with the normal area of the plane

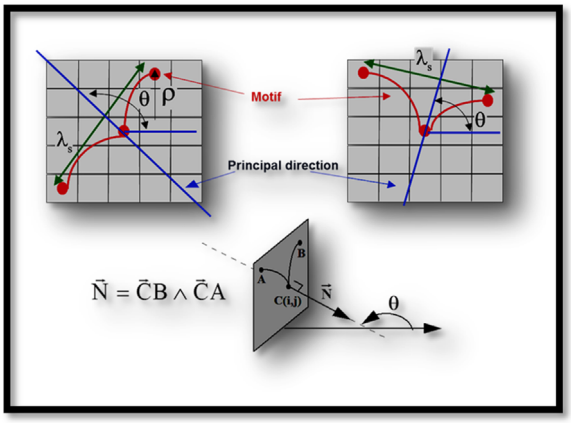

Fig. 7. Local detection of the motif direction.

determined by the three elements of the motif illustrated in Fig. 7, if the first summit is point A, point C is the pit, and the second summit is point B. The direction of the motif is collinear within the limits of the normal $\vec{N}$ which is given by the vectorial product:

$$\vec{N} = \quad \vec{CB} \wedge \vec{CA} \tag{18}$$

So that the motif direction to coincide with the of a principal of the trajectory of the abrasive groove composed of a succession of motifs, we need to know if the pit point $C(i,j)$ which is related to the orientation of neighbouring pits; this is obtained by determining the intersection between a half straight from $B(i,j)$ and the nearest pits. If there is an even number of points, pit $C(i,j)$ is not within the orientation of the groove. Otherwise it is definitively within the orientation of the principal valley.

The application of this algorithm on the set of abrasion grooves can reconstruct the family distribution density of motifs in each direction. The results of the statistical analysis are shown in the Fig. 8, the average values of the abrasion parameters are presented in terms of deformation, contact time, the mean and maximum of the friction ploughing component. It may be noted that the anisotropy is instead marked for the deformation parameter and the contact time. The anisotropy of the deformation coefficient of friction is very pronounced for the surface S3.

2.5. Multi-scale decomposition of honed surfaces by 2D continuous wavelet

In this abrasion finishing problem, it is in a multi Tribology - contact between the abrasives of different sizes and the cylinder surface. The signing of finishing by honing include several scales of surface patterns. To compare the surfaces of four surfaces in a wide range of scale, it is necessary to study in detail the effect of process parameters in several spatial scales

A multi-scale analysis developed in this part of work allows the decomposition of topographic surfaces into different roughness scales. This decomposition used 2D continuous wavelet transform.

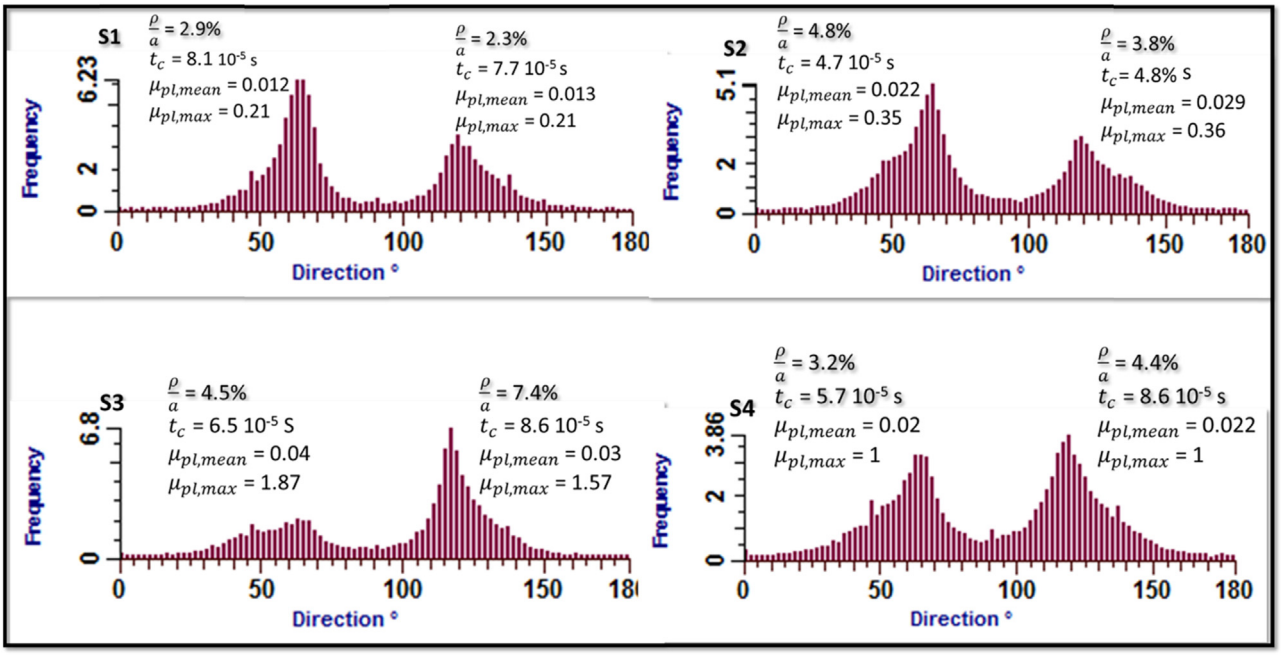

Fig. 8. Effect of honing angle on abrasive parameter.

It is applied in order to quantify the manufacturing effect on all the full range of wavelengths, from roughness [20–27].

The continuous wavelet transform can be interpreted as a multi-channel filter system. The surface topography components pass through a filter bank which is a set of the contracting wavelets.

The continuous wavelet transform of a two dimensional space function $f(\boldsymbol{X})$, is given by:

$$W_{\psi}f(\boldsymbol{b}, a) = \int_{-\infty}^{+\infty} f(X)\overline{\psi_{a,\vec{b}}}(\mathbf{X})\, \mathrm{d}\, \boldsymbol{X} \tag{19}$$

Where $W_{\psi}f(\boldsymbol{b},a)$ is the wavelet coefficient, $\boldsymbol{X}=(x, y)$ is the spatial position, the over bar denote complex conjugate, and $\psi_{a,\boldsymbol{b}}(\mathbf{X})$ for this two –dimensional domain is given by:

$$\psi_{a,\boldsymbol{b}} = \frac{1}{a}\psi\left(\frac{\boldsymbol{X}-\boldsymbol{b}}{a}\right) \tag{20}$$

Where $\psi(\boldsymbol{X})$ the mother wavelet, b is the translation parameter, and a is a scale spatial parameter. The normalisation constant 1/a, is defined such that the total energy of the analysing wavelet is independent of the scale:

$$\int_{-\infty}^{+\infty} \left|\psi_{a,\boldsymbol{b}}(\boldsymbol{X})\right|^2 \mathrm{d}\, \boldsymbol{X} = \int_{-\infty}^{+\infty} |\psi(\boldsymbol{X})|^2 d\boldsymbol{X} \tag{21}$$

For all values of a.

The number of wavelets corresponds to the number of iterations.

In this first analysis we use the "hat Mexican-2D" wavelet given by the following expression:

$$\psi(x, y) = (2-r)\exp\left(-\frac{r}{2}\right) \tag{22}$$

With $r = \left(x^2 + y^2\right)^{1/2}$

It's an isotropic radial and symmetrical wavelet which satisfies the existence conditions [5]. It has two vanishing moments and admits good localization properties at the same time in the space field and the frequencies domain.

The result of the decomposition makes it possible to identify the component of the surface at each scale after a 2D inverse wavelet transformation.

The Inverse 2D Continuous Wavelet Transform is defined by:

$$f(x, y) = \frac{1}{C_g}\int_{-\infty}^{+\infty}\int_{-\infty}^{+\infty}\int_{-\infty}^{+\infty}\int_{-\infty}^{+\infty} W_{b,a}^{f}(x, y)\psi_{a,b}(x, y)\frac{db_x db_y da_x da_y}{a_x^2 a_y^2} \tag{23}$$

With $C_g = \int_{-\infty}^{-\infty}\int_{-\infty}^{+\infty}\frac{|\Psi(u,v)|^2}{uv}dudv$

For Mexican Hat wavelet is approximately equal to 3.541.

The continuous wavelet transform can be interpreted as a multi-channel filter system. The surface topography components are analyzed through a filter bank which is a set of the contracting wavelets. The number of wavelets corresponds to the number of iterations, because the wavelet is a function of contracting coefficient "a" [22]. The result of the decomposition makes it possible to identify the various scales after a 2D inverse wavelet transformation. In each spatial scale, we can quantify the different geometric parameters of the grounds and the different abrasion parameters, Fig. 9.

The results of multi-scale analysis of the 4 surfaces are shown in Figs. 10 and 11. Is shown in this analysis the multiscale evolution of deformation $\frac{\rho}{a}$ and the volume rate of wear V_{abr} .

The results are presented in a comparative manner with respect to the surface S1. It may be noted that the surface S1 contains honing scratches with less deformation and with a low abrasion volume in a wide range of scale.

2.6. Fractal analysis and multi-scale study

Our analysis is focused on the irregularity of the surface roughness generated by honing, whose texture exhibits fractal properties. As shown in many works in the literature [28–36] several machining processes lead to surfaces having this kind of properties. In particular, Majundar and Bushan [28,29] reported that processes producing deterministic texture do not yield self-

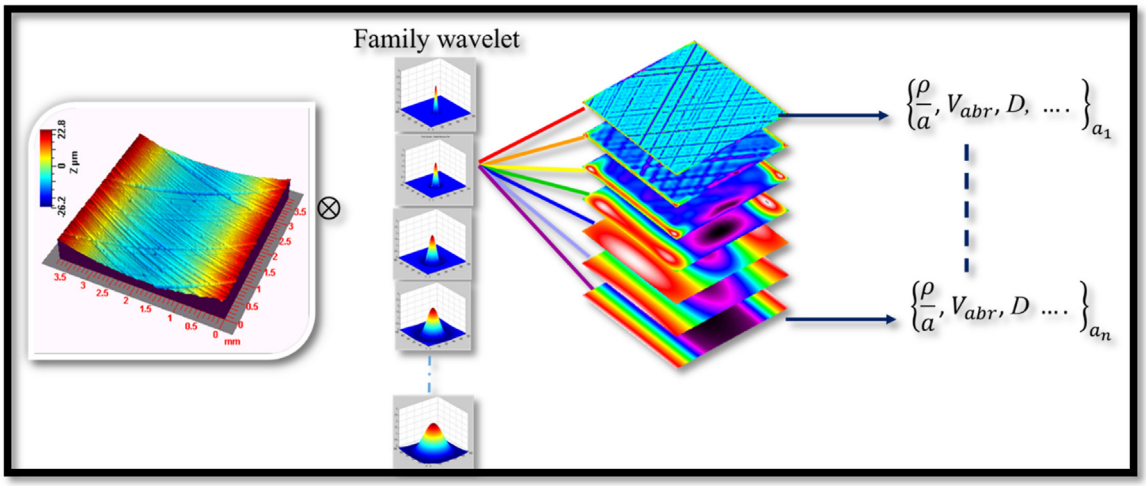

Fig. 9. Multi-scale analysis by continuous wavelet transform of honed surface.

affined fractal surfaces, whereas those producing random textures do. The basic properties of self -affinity are presented in more details in Felder's book [30] and can be defined as below:

A motif of depth *Z(x)* is self-affined if it is (statistically) invariant under the affined transformation:

$$\left\{\begin{matrix} x \to \lambda x \\ Z(x) \to \mu Z(x) \end{matrix}\right\} \tag{24}$$

the group properties imply that μ should be homogeneous function of λ. The homogeneity index H such that

$$\mu = \lambda^{H} \tag{25}$$

is the roughness Hurst exponent or Hölder condition, with $0 < H \leq 1\,0$. Let us note that for a self-similar invariance, H is unity. In this case, both scaling factors are equal.

The details of Z(x) depend on the length scale, we assume each realization of Z(x) to be a continuous, but non differentiable function. It means that the presence of any small roughness elements may prevent us from reaching a satisfactory limit of

$$\frac{(Z(x+\Delta) - Z(x))}{\Delta} \text{as } \Delta \to 0. \tag{26}$$

A simple way to obtain this behavior for a function Z(x) is to assume that the increment of Z(x) is related to Δ by the self-affinity relation:

$$|Z(x+\Delta) - Z(x)| \propto \Delta^{H},\ 0 < H < 1\ \Delta \to 0. \tag{27}$$

$\lim_{\Delta \to 0} \Delta^{H-1}$, only exists if H = 1.

The derivative of Z, which is proportional to the limit

For 0 < H < 1, this derivative is infinite, although the function

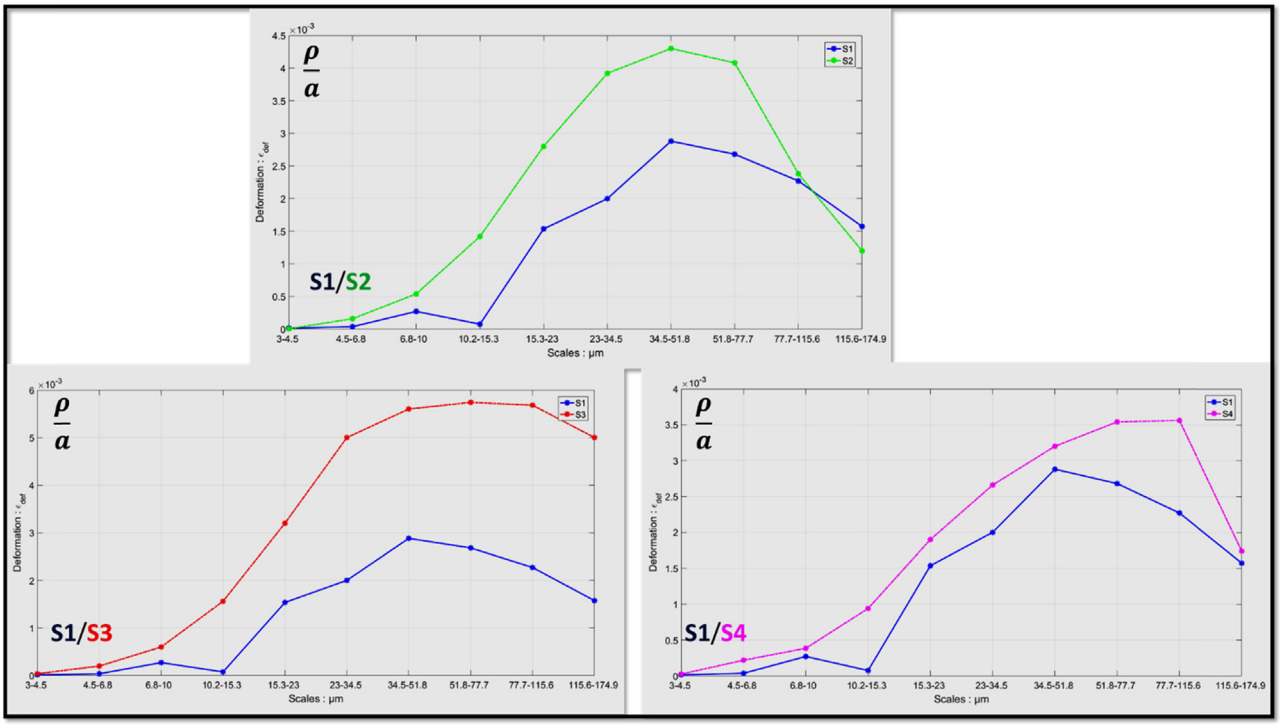

Fig. 10. Multi-scale comparison of deformation: $\frac{\rho}{a}$.

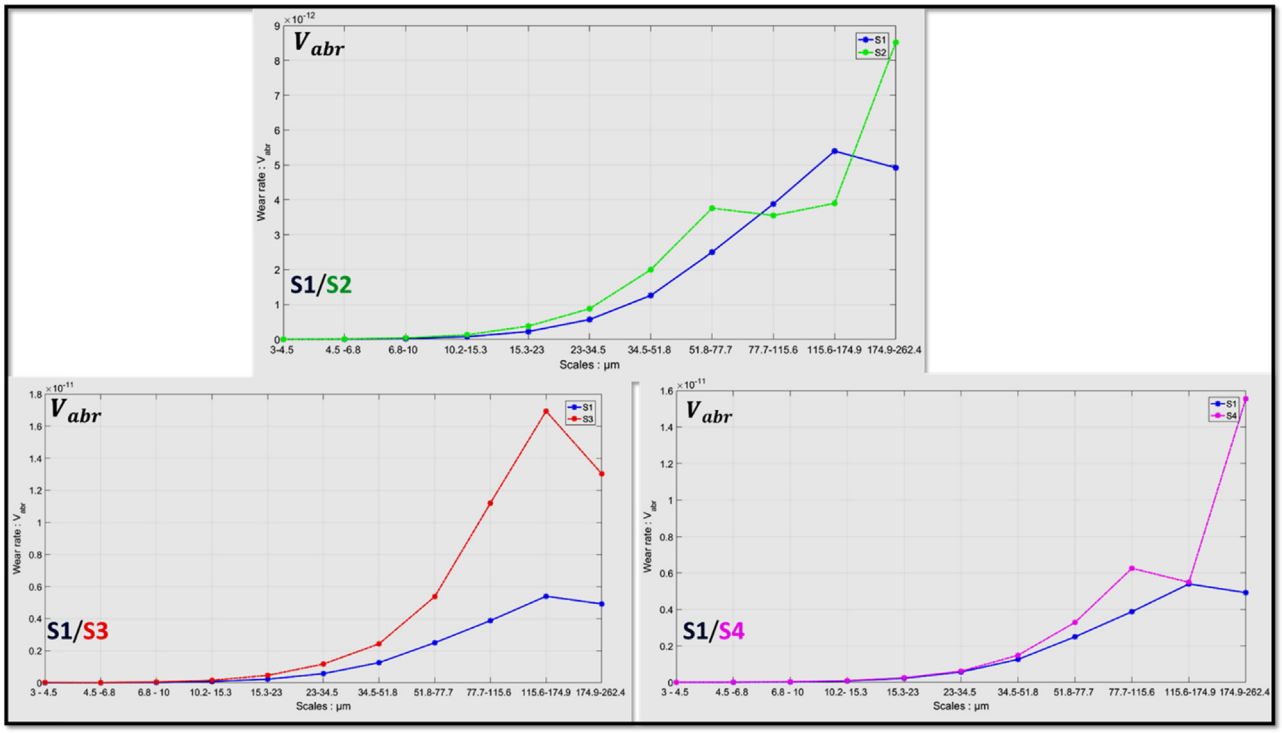

Fig. 11. Multi-scale comparison of wear volume of abrasion: V_{abr}.

remains continuous, and for H=0 the function itself becomes discontinuous. So by varying from 0 to 1, the parameter H characterizes the transition from a non-continuous to differentiable function, the range $0 < H < 1$ corresponding to non- differentiable functions which become smoother as H increases. Thus H can be considered as an indicator of roughness.

The fractal dimension of rough surface defined as $D=3-H$, have the interesting property of being locally affine, then they may be stationary a large scale. The determination of the fractal dimension of a rough surface, is described in great detail in [37,38].

The analysis of the fractal dimension was performed on ten scale from the multi-scale analysis. It may be noted that the surface S1 has the highest fractal dimension on eight scales.

The fractal dimension of the surface S2 which took a single finish with abrasive grain size of 100 µm, decreases after four spatial scales. the effect of the double finishing of surfaces S3 and

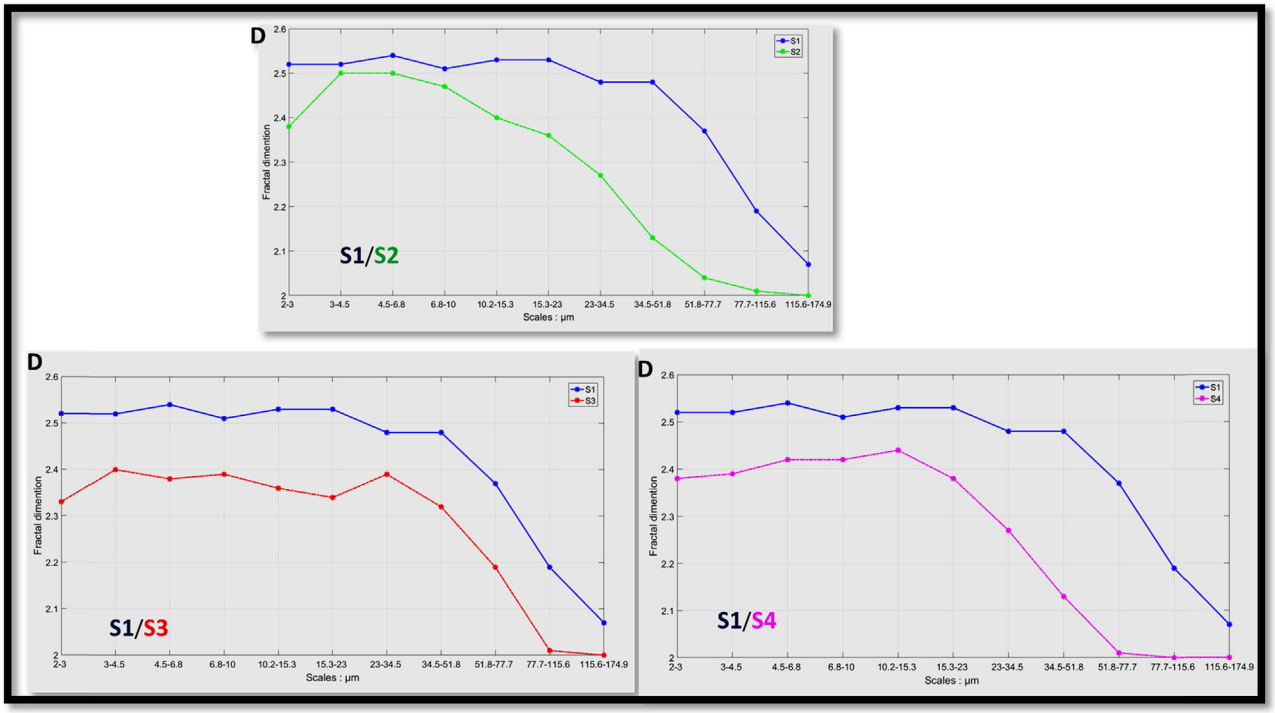

Fig. 12. Multi-fractal analysis of honed surfaces.

S4 results with finishing parameters (cutting speed and frequency of the oscillations) have smaller fractal dimensions than the surface area S1 in all spatial scales.

As a consequence of an important fractal dimension of the surface S1 (D=2.5) on a large scale, allows this surface a significant retention of lubricant volume and reduced wear during the life of the cylinder liner, Fig. 12.

3. Conclusion

In the technical processing literature, Honing is used to describe a process in which a produced finished surface with desired geometry and improved multi-scale tribological performances (low friction, near zero running-in wear, high oil retention capacity, high load carrying capacity, etc.) is the objective. To move this forward, a hybrid approach, where the existing theoretical models should be modified based on experimental results, should be taken to develop appropriate multi-scale methods for accurate predictions that inform the design of optimized honing process. This paper introduces an attractive mixed approach for a multi-scale analysis of a criss-cross scratch pattern produced by abrasive honing. This approach demonstrates firstly that honing is constant-force grinding process where the abrasive grains act as multi-indenter that requires contact force and deformation by friction component, which essentially depend on the size and geometry of abrasive grains. Secondly, the morphological quantification based on motifs decomposition is used a powerful tool to assess how surface finish produced by honing is affected not only by the complication of the kinematics of abrasive grits (abrasive sticks are loaded against the work and simultaneously rotated, oscillated axially with radial expansion) but also depends heavily on the contact conditions and working variables of honing (contact geometry, load, speeds, temperature, material, etc.). The main conclusion in surface finish features produced by honing is summarized next.

- The surface finish S1 produced by tow honing successive steps (first rough honing step: (110 μm, Vc=50 m/min) followed by second finish honing step: (30 μm, Vc = 32 m/min), pressure 5 bars and 5 oscillations) shows the optimal honing configuration.
- The honing process parameters of the optimum surface S1 exhibit contact conditions of less deformation and abrasive volume, low coefficient of wear and low Peclet number ($\phi < 0.2$).
- The multi-fractal dimension that describes the uniformity of abrasion scratches pattern and the ability of honing to produce surface finish with high volume of oil retention.
- The new hybrid multi-scale approach permits for the first time the study of the Achard's law in large scale of space and time.
- The morphological parameters and the mechanical criteria defined in this work allow simultaneously the quality assessment of the produced finish by honing as well as its working variables which make it possible to reproduce an equal quality of surface finishing, while controlling the geometric quality of the abrasive grains in a large length of scale of abrasive scratches.

References

[1] J. Lee, S. Malkin, Experimental Investigation of the Bore Honing Process, 115, ASME, New York, 1999, p. 406.
[2] T.K. Puthanangady, S. Malkin, Experimental investigation of the superfinishing process, Wear 185 (1995) 173–182.
[3] T. Ueda, A. Yamamoto, An analytical investigation of the honing mechanism, J. Eng. Ind. 106/237 (1984).
[4] H. Weule, Improved honing through process control, Ann. CIRP 37/1 (1998).
[5] E. Salje, M. Von See, Process optimization in honing, Ann. CIRP 36/1 (1987).
[6] T. Sasaki, K. Okamura, The cutting mechanism of honing, Jpn. Soc. Mech. Eng. 2 (5) (1959).
[7] A.M. Gouskov, A.S. Voronov, A. Eric, C. Subhash, Simulation of machined surface formation while honing, in: ASME International Mechanical Engineering Congress and Exposition, Anaheim, California USA, 2004.
[8] A.M. Gouskov, S.A. Voronov, E.A. Butcher, Influence of honing dynamics on surfaceformation, in: 2003, DETC 03, ASME Design Engineering Technical Conferences and Computers and Information in Engineering Conference, Chicago, Illinois, USA, Sept 2–6, 2003.
[9] D. Bardac, I.D. Marinescu, Surface Generation in the case of honing with superabrasives, Society of Manufacturing Engineers, Technical Paper MR99-240, 1999.
[10] A.A. Torrance, The effect of grit size and asperity blunting on abrasive wear, Wear 253 (2002) 813–819.
[11] J. Larsen-Badse, Influence of grit size on the groove formation during sliding abrasion, Wear II (1968) 213–222.
[12] R. Gahlin, S. Jacobson, The particle size effect in abrasion studied by controlled abrasive surfaces, Wear 22 (1999) 118–125.
[13] J.L. Bucaille, E. Felder, L'essai de rayure sur polymères et métaux, Matériaux et Techniques, N° 3, 2001, pp. 29–44.
[14] J.F. Archard, J. Appl. Phys. 29 (1953) p981.
[15] A. Kapoor, K.L. Johnson, J. Williams, Wear, 175 (1995) 81–82.
[16] K. Peucker, D. Douglas, Detection of surface specific points by local parallel processing of discrete terrain elevation data, Comput. Graph. Image Process. 4 (1975) 375–387.
[17] H. Zahouani, Spectral and 3D motifs identification of anisotropic components. Analysis and filtering of anisotropic patterns by morphological rose approach, in: Proceedings of the 7th International Conference on Metrology and Properties of Engineering Surrfaces, Göteborg, 1997, pp. 220–230.
[18] H. Zahouani, et al., The morphological tree transform of surface motifs, Int. J Mach. Tools Manuf. 41 (2001) 1961–1979.
[19] D.K. Srivastava, A.K. Agarwal, J. Kumar, Effect of liner surface properties on wear and friction in a non-firing engine simulator, J. Mater. Des. 28 (2007) 1632–1640.
[20] I. Daubechies, The wavelet transform, time-frequency localization and signal analysis, IEEE Trans. Inf. Theory 36 (5) (1990) 961–1005.
[21] A. Cohen, J. Kovacevic, Wavelets: the mathematical background, Proc. IEEE 84 (4) (1996).
[22] Chen, J. Raja, S. Simanapalli, Multi-scale of Engineering Surface, Int. J. Mach. Tools Manuf. 35 (2) (1995) 231–238.
[23] D. Wolf, R. Husson, Application des ondelettes à l'analyse de texture et à l'inspection de surface industrielle, J. Phys. III Fr. 3 (1993) 2133–2148.
[24] S.H. Lee, H. Zahouani, R. Caterini, T.G. Mathia, Morphological characterization of engineered surfaces by wavelet transform, Int. J. Mach. Tools Manuf. 38 (5–6) (1998) 581–589.
[25] H. Zahouani, S.-H. Lee, R. Vargiolu, The multi-scale mathematical microscopy of surface roughness. Incidence in tribology, Lubr. Front. Elsevier Sci. B.V. (1999) 379–390.
[26] H. Zahouani, S.H. Lee, R. Vargiolu, J. Rousseau, Characterization of surface topography by continuous wavelet transform, Acta Phys. Superf. IV (2001) 1–23.
[27] M. El Mansori, S. Mezghani, L. Sabri, H. Zahouani, On the concept of process signature in the analysis of multi-stage surface formation, Surf. Eng. 26 (8) (2010) 216–223.
[28] A. Majumdar, B. Bhushan, Fractal model of elastic-plastic contact between rough surfaces, ASME J. Tribol. 113 (1991) 1–11.
[29] B. Bhushan, A. Majumdar, Elastic-plastic contact model of bifractal surfaces, Wear 153 (1992) 53–64.
[30] J. Feder, Fractals, Plenum Press, New york, 1988.
[31] B. Mandelbrot, Self-affine fractals and fractal dimension, Phys. Scr. 32 (1985) 257–260.
[32] B. Mandelbrot, J.W. Van Ness, Fractional Brownian motions, fractional noises, and applications, SIAM Rev. 10 (1968) 422–437.
[33] John C. Russ, Fractal surfaces, Plenum Press, New york, 1944.
[34] D. Saupe, H.O. Peitgen, The Science of Fractal Images, Springer-Verlag, New York, 1988, pp. 82–91.
[35] John C. Russ, Fractal Surfaces, Plenum Press, New york, 1994.
[36] D. Saupe, H.O. Peitgen, The Science of Fractal Images, Springer-Verlag, London, 1988, pp. 82–91.
[37] H. Zahouani, R. Vargiolu, J.-L. Loubet, Fractal models of surface topography and contact mechanics, Math. Comput. Model. 28 (4–8) (1998) 517–534.
[38] C. Vallet, D. Lasseux, P. Sainsot, H. Zahouani, Real versus synthesized fractal surfaces: contact mechanics and transport properties, Tribol. Int. (2009).
[39] K. Kato, in: I.M. Huthings (Ed.), New directions in Tribology, Mech. Eng. Publ., London, 1997, pp. 125–135.
[40] M. Yousfi, S. Mezghani, I. Demirci, M. El Mansori, Tribological performances of elliptic and circular texture patterns produced by innovative honing process, Tribol. Int. 100 (2016) 255–262.